Editors' Suggestion

Desktop laboratory of bound states in the continuum in metallic waveguide with dielectric cavities

Evgeny Bulgakov, Artem Pilipchuk, and Almas Sadreev*
Kirensky Institute of Physics, Federal Research Center KSC SB RAS, 660036 Krasnoyarsk, Russia

(Received 13 May 2022; revised 24 July 2022; accepted 26 July 2022; published 16 August 2022)

We consider dielectric cavities whose radiation space is restricted by two parallel metallic planes. The TM solutions of the Maxwell equations of the system are equivalent to the solutions of periodical arrays of dielectric cavities. The system readily allows to achieve bound states in the continuum (BICs) of any type including topological BICs as dependent on position and orientation of the cavities relative to the planes and that extremely facilitates experimental studies in comparison to infinite arrays of the cavities. We show the effect of merging of topologically protected BICs that pushes the square asymptotic of the Q factor into the power degree 4 or even 6.

DOI: 10.1103/PhysRevB.106.075304

I. INTRODUCTION

Since the famous paper by Gustav Mie [1] engineering of dielectric cavities in optics and photonics has been a long-standing area of implementation various ideas and approaches to enhance the quality factor Q due to its paramount importance in both applied and fundamental research. Conventionally, light can be confined in closed or Hermitian system where access to radiation channels is prohibited due to, for example, metallic covering or embedding the resonant frequencies of cavity into band gap of photonic crystal [2]. However, that conflicts with necessity of easy manipulation of light confined in the cavity. On the other hand, although the compact dielectric resonator is in air, its Q factor is very restricted due to embedding into the radiation continuum whose spectrum is given by light cone $\omega = ck$ with no cutoff. In principle the problem can be solved cardinally, if addressed to infinitely long periodical structures, for example, gratings. The periodicity quantizes the directions of radiation leakage by means of diffraction orders and brings cutoffs. As a result, the periodical structures support bound states in the radiation continuum (BICs) [3–16]. However, in practice, increasing the number of cavities in periodical arrays is limited by material losses [17] and structural fluctuations [18]. Moreover grating slabs yield isolated dielectric cavities in compactness. In view of that breakthrough in the engineering of dielectric cavities was achieved owing to avoided crossing of resonances of single cavity [19–23] or different cavities [24,25].

In spite of reporting unprecedent values of the Q factor in these cavities that cannot achieve infinity because the isolated cavity in air cannot support the true BICs [26,27]. In other words, although the multipolar radiation with low orders of orbital momentum can be suppressed due to avoided crossing of resonances the higher order multipolar radiation still remains [23,24,28,29]. In the present paper we propose a compromise solution of the problem by restriction of radiation space by two parallel metallic planes separated by a distance d. Then, for instance, the single dielectric cylinder inserted between the planes, as depicted in Fig. 1(a), is equivalent to the infinite periodical array of cylinders with the period d in which BICs were considered by many reports [7,10,12,13,16,30–36]. The equivalency follows from the Dirichlet boundary conditions at perfectly conducting metal surface for the TM solutions of the Maxwell equations. Two identical cavities between the planes are, respectively, equivalent to two periodical arrays of rods which support Fabry-Perot BICs [8,37].

Moreover, the case of metallic waveguide of rectangular cross section allows to remove another typical theoretical approximation of infinitely long cylinders rods as shown in Figs. 1(a)–1(d). Examples of equivalent arrays of dielectric cavities are sketched in Fig. 2. Thus, the metallic waveguide with one or two dielectric insets is converting into desktop laboratory of variety of BICs. While achievement of the BICs in gratings often requires tuning of geometrical parameters, the present case of desktop laboratory allows to achieve the BICs by simple variation of the waveguide's width, position, or orientation of dielectric inset inside the waveguide. However, the main advantage of this laboratory is related to material losses and structural fluctuations, which fast saturate growth of the Q factor with the number of cavities in periodic arrays [17,18,38] that prevents to clearly unveil the BICs.

The existence of symmetry protected (SP) BICs near rigid symmetric obstacle cylinder placed symmetrically in between parallel walls with Neumann or Dirichlet boundary conditions imposed upon them was proven in the literature [39–41]. Thereafter, Linton *et al.* [42] and Duan *et al.* [43] have examined the cases of accidental BICs for slender rods of arbitrary cross section placed nonsymmetrically in waveguide. We develop these results for the case of dielectric rods of circular and rectangular cross section and find a threshold for dimensions and permittivity of the rod below which the BICs do not exist. Once the rod is shifted relative to center line we obtain equivalent dimerised chain of rods as shown in

*Corresponding author: almas@tnp.krasn.ru

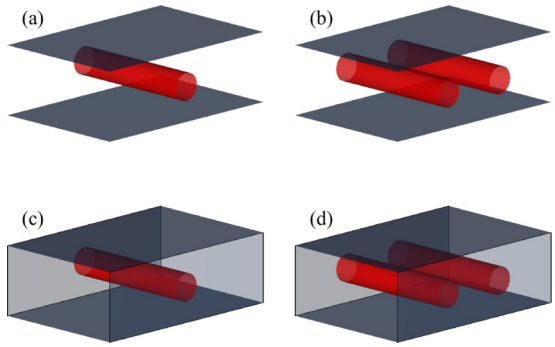

FIG. 1. Single (a) and two parallel (b) infinitely long dielectric cylinders between two metallic planes. The same for cylinders of finite length inside waveguide of rectangular cross section [(c),(d)].

Fig. 2(c). There are only a few reports of BICs in dimerised arrays of dielectric cavities [44,45]. Moreover, the rectangular rod inserted between metallic planes brings new parameter to vary, the angle of orientation of the rod as shown in Fig. 2(d). That, in turn, opens a way for realization of topologically protected BICs with winding numbers $m = \pm 1$ in two-parametric space of angle and frequency or angle and distance between rods.

II. CYLINDER BETWEEN TWO METALLIC PLANES

We start by considering single dielectric cylinder of the radius R inserted parallel to metallic planes as depicted in Fig. 1(a). In what follows all quantities are measured in terms of the distance between plates d with x axis is directed along the waveguide and z axis is directed along the rod. Because of boundary conditions for the electric field $E_z(x = 0, d) = 0$ the solutions of the Maxwell equations of the system are equivalent to the solutions in periodical infinite array of rods at the Γ or X point as sketched in Fig. 2(a).

There are two distinct cases for these solutions. The case of dielectric inset symmetrically disposed between two parallel metallic planes is equivalent to periodical array of rods with the period d as shown in Figs. 2(a) and 2(b). Figure 2(c) presents the case of cylinder shifted from the center line of waveguide by distance Δ. Then the TM solutions of the system coincide with the solutions of the binary array of cylinders with double period $2d$. The equivalence of the solutions allows us to use well-known analytical approaches developed

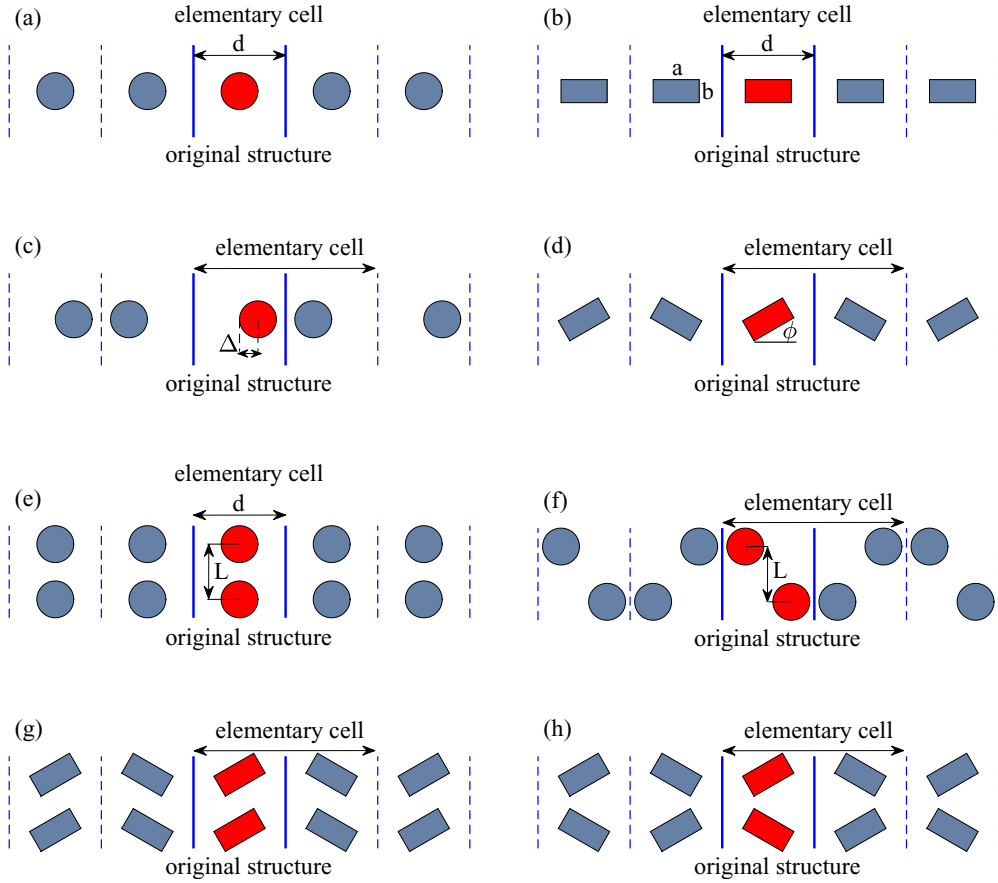

FIG. 2. Periodical arrays of dielectric rods whose solutions at the Γ point are equivalent to the solutions of Maxwell equations of rods placed between two parallel metallic planes shown by solid-thick lines. The original rod is shown by red while its images at metallic planes are shown by gray. Cylindrical (a) and rectangular (b) rods positioned symmetrically between planes are equivalent to the periodical array of rods with period d. Cylindrical rod shifted by distance y_0 from center line (c) and rectangular rod rotated by the angle ϕ makes the system equivalent to dimerised chain. (e) Two rods positioned symmetrically make the system equivalent to double array of rods which can support FPR BICs. Two circular rods, positioned nonsymmetrically (f) or two rotated rectangular rods (g) and (h) are equivalent to two dimerised chains.

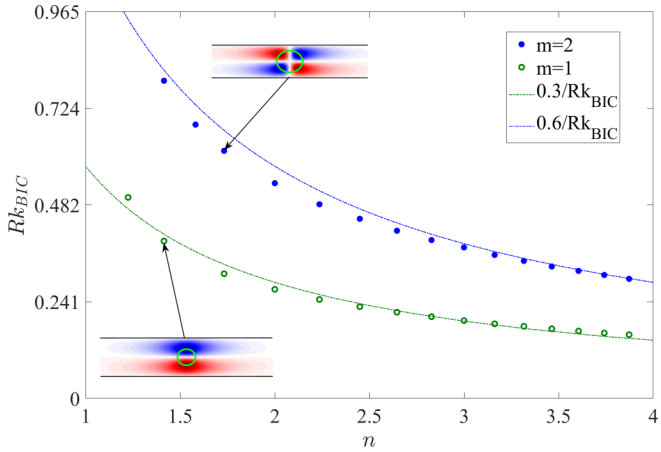

FIG. 3. Curves of existence of the SP BICs vs refractive index and radius of circular rod. Insets show patterns of SP BICs (electric field E_z).

for periodical arrays of dielectric resonators [46,47]. We complement these approaches by COMSOL MultiPhysics numerical calculations for the rods of circular and rectangular cross sections.

In Fig. 3 we show typical examples of the SP BICs with azimuthal indices $m = 1$ and $m = 2$ for the case of symmetrical position of dielectric cylinder with the refractive index n [Fig. 2(a)]. It is clear that in order the dielectric rod could trap the EM wave with definite wavelength $\frac{2\pi}{k}$ its radius R has to be comparable with the characteristic wavelength inside the rod $\frac{2\pi}{nk}$. Therefore the curve of existence of the SP BICs can be evaluated as $Rnk_{BIC}(n, R) \approx 1$. Numerical behavior and comparison with this evaluated formula is shown in Fig. 3. Since the diameter of rod cannot exceed distance between mirrors we obtain that BICs cannot exist for $nk_{BIC} \geqslant 2$. For nonsymmetric position of the rod inside the waveguide the SP BICs transform to accidental BICs at tuned rod's radius or refractive index. In the equivalent system of binary periodical array of rods [see Fig. 2(c)] these BICs correspond to the BICs at Γ point. Phase diagrams of existence of the accidental BICs are plotted in Fig. 4.

III. RECTANGULAR ROD BETWEEN TWO METALLIC PLANES

First of all, the rectangular rod is interesting; Linton *et al.* [42] have shown existence of accidental BICs under assumption that the aspect ratio a/b is sufficiently large and the rod is metallic. Moreover, rectangular rod brings new parameter to vary, rotation angle relative to the frame of metallic waveguide as shown in Fig. 2(d). Figure 5(a) shows curves of accidental BICs versus dimensions of rectangular quartz rod $a \times b$. Insets show evolution of two accidental BIC modes (electric field E_z directed along the rod). In fact, there are more curves, which differ by number of nodal lines cross to the waveguide. TM propagating channels are given by simple formula $k^2 = k_x^2 + \pi^2 p^2$, $p = 1, 2, 3, \ldots$ where k_x is the wave vector of TM waves along the waveguide. We consider only the BICs embedded into the continuum of the first propagating

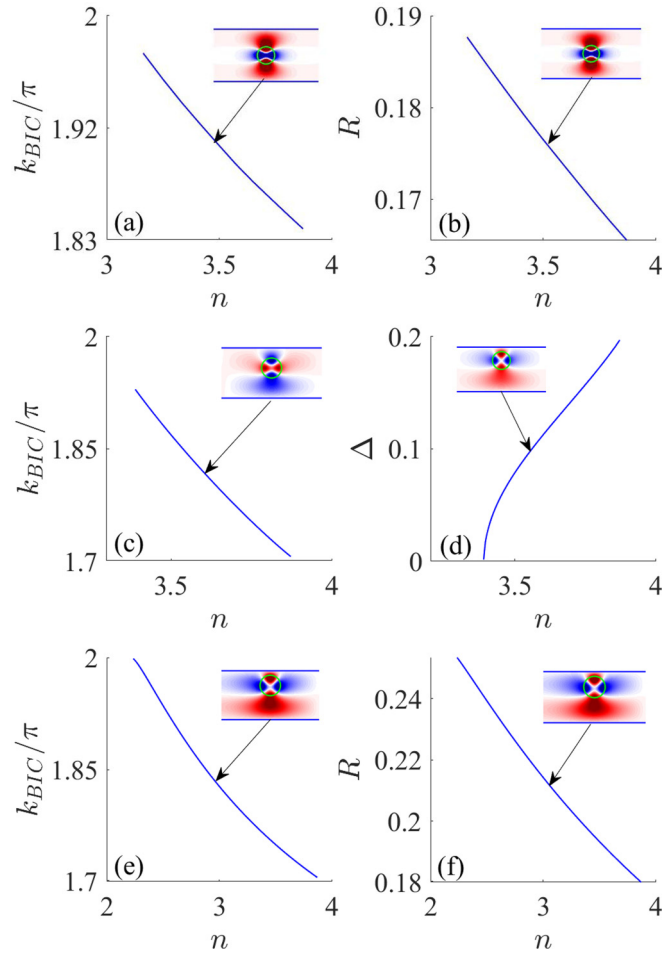

FIG. 4. Curves of existence of accidental BICs in two-parametric space of refractive index of the rod and (a) frequency, (b) radius of the rod for $\Delta = 0$; (c) frequency, (d) displacement of the rod for $R = 0.18$; (e) frequency, (f) radius of the rod for $\Delta = 0.3$. Insets show the accidental BICs for certain parameters.

channel of the waveguide with $p = 1$ and frequencies below the cutoff of the second propagating channel $\pi < k < 2\pi$.

First, one can see that the curves of BICs follow the analysis of Linton *et al* obtained by different mathematical techniques [42] for the case of Dirichlet BC at the walls of rectangular rod, i.e., metallic rod. These accidental BICs shown in Fig. 5(a) have clear physical origin. Far from the rod, accidental BICs follow the evanescent mode $p = 2$, which is orthogonal to the first propagating channel $p = 1$ and therefore cannot go out. The dielectric rod perturbs the evanescent mode and the perturbation strength depends on size and refractive index of the rod. The more the index and size, the more perturbation. In spite of difference between the metallic and dielectric rods, the accidental BIC exists at $b \to 0$. However, BIC's frequency is limited by the cutoff 2π of the second channel and the localization range diverges for $k \to 2\pi$ as insets in Fig. 5(b) show.

IV. FABRY-PEROT BICS: TWO RODS INSIDE WAVEGUIDE

Two identical circular rods inserted symmetrically inside the waveguide as shown in Fig. 1(e) make the system

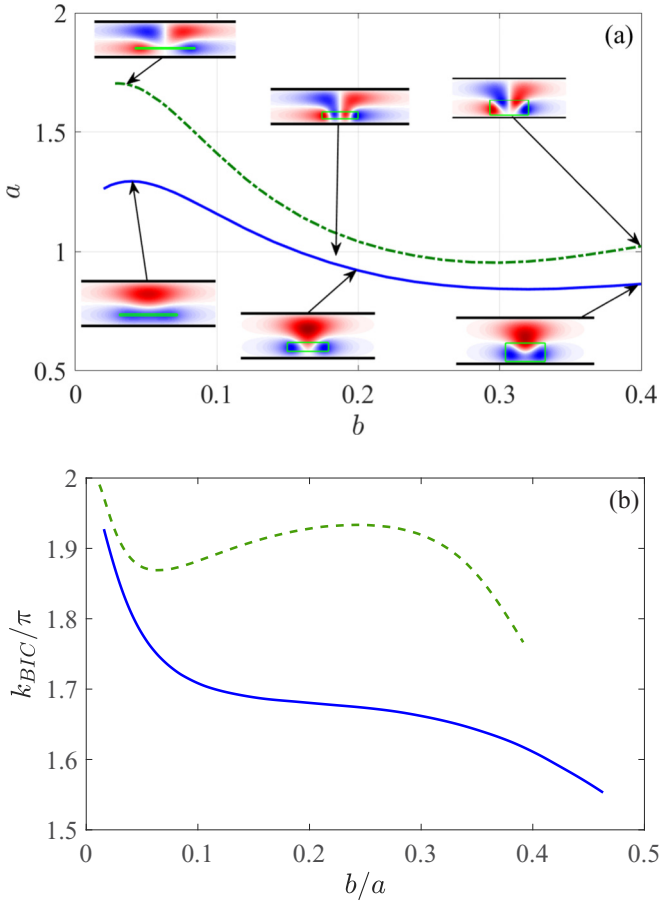

FIG. 5. Curves of existence of the accidental BICs. (a) As dependent on cross section of rectangular quartz rod $a \times b$ at $\Delta = 0.25$ with refractive index $n = 2.05$. (b) The frequency of BICs vs aspect ratio of rectangular rod.

equivalent to periodic double arrays of subwavelength dielectric cylinders. Such arrays were studied by Ndangali and Shabanov with analytic TM solutions for BICs in the limit of thin cylinders [37]. Underlying physical mechanism for BICs is the Fabry-Perot one [48] in which each array perfectly reflects electromagnetic waves at definite frequency k_c. Then, two arrays serve as ideal mirrors, which are able to capture electromagnetic wave with frequency k_c at discrete distances roughly equal to integer number of half wavelength π/k_c. Figure 6 demonstrates the effect of total reflection of TM waves by (a) cylindrical and (b) rectangular rods positioned symmetrically inside the waveguide. The effect of total reflection by rod inserted into waveguide exists irrespective to position of the rod inside the waveguide. In Fig. 6(b) one can see the well-known effect of collapse of Fano resonance for $\phi \to 0$ and $\Delta = 0$ at which the scattering function tends to the SP BIC [49]. Figure 6(c) shows that total reflection ($T = 0$) is achieved owing to variation of cylindrical rod radius. However, the variation of the rod size is difficult in the experiment. Figure 6(d) demonstrates that the problem can be easily solved by orientation of rectangular rod relative to waveguide.

In Fig. 7(a) we show results of numerical calculations for the case of two circular quartz rods inserted symmetrically [see Fig. 2(c)] with patterns of Fabry-Perot BICs for different

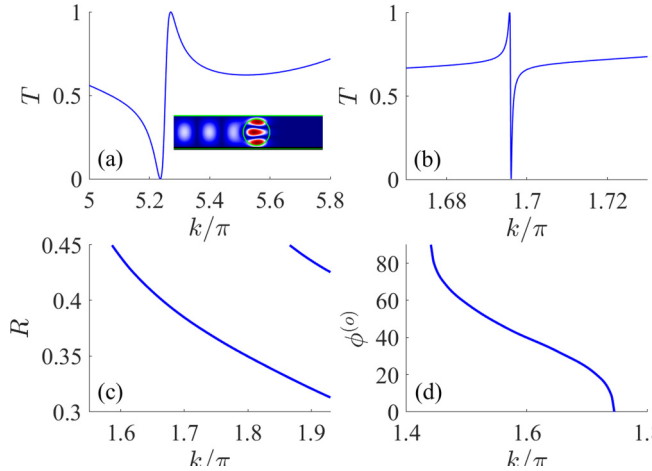

FIG. 6. Transmittance vs frequency (upper panels) for (a) cylindrical rod with $R = 0.4$, $\Delta = 0$, (b) rectangular rod with cross section 0.6×0.3 and $\Delta = 0.01$. Transmittance zeros (bottom panels) vs frequency of incident wave and (c) radius of cylindrical rod, (d) orientation angle of rectangular rod for $\Delta = 0$. The refractive index of the rods is $n = 2.05$ in all cases.

distances between cylindrical rods. That case is equivalent to the case of two periodic arrays considered in Refs. [37,50]. It is interesting that similar type of BICs exist even for nonsymmetrical position of circular rods an one can see from Fig. 7(b). In Fig. 8 we show curves of the Fabry-Perot BICs in two-parametric space of the rotation angle of rods ϕ and distance between them L for two distinct cases of rods rotation: in-phase and antiphase.

One of the ways to experimentally confirm BICs is observation of singularities in the wave transmission in waveguide. At the BIC point the total reflection coalesces with the full transmission [51], which can be defined as collapse of Fano resonance [49]. In Fig. 9 we present typical examples of such singular points in parametric space of incident light frequency and orientation angle of rectangular rods. Moreover, one can see that the transmission peaks follow the resonant frequencies of the system shown by solid lines in Fig. 9. There are two equivalent cases $\phi = 0$ and $\phi = \pi/2$, which were considered in Refs. [8,52]. In both cases we observe two solutions for BICs whose frequencies are considered as splitting due to interaction of rods. As a result we obtain the symmetric and antisymmetric hybridized solutions shown in insets of Fig. 9. If the rods were in air the splitting of frequencies would decrease as $1/L^2$ [53]. However, the presence of parallel metal

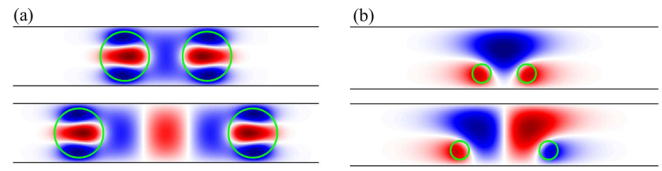

FIG. 7. Patterns of Fabry-Perot BICs for the case of two cylindrical rods (shown by green circles) positioned (a) symmetrically ($R = 0.4$, $n = 2.05$) and (b) shifted across to the waveguide inside the waveguide by $\Delta = 0.25$, $R = 0.15$.

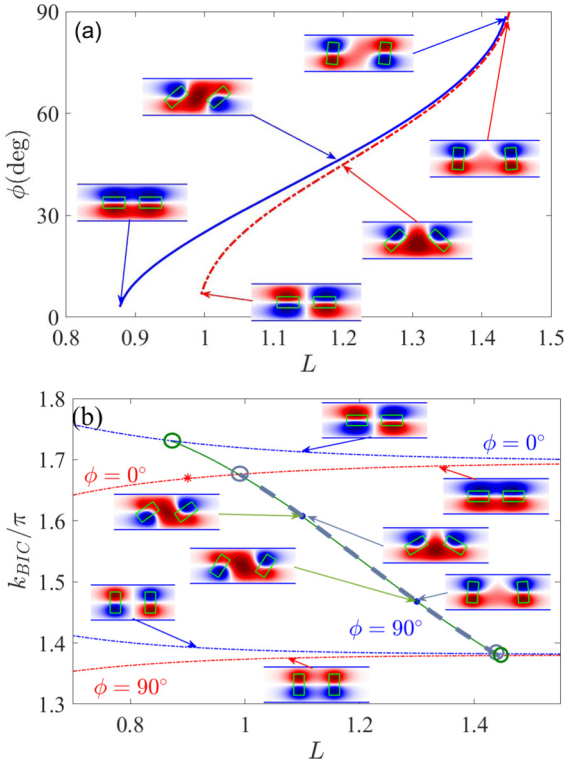

FIG. 8. Curves of existence of topologically protected BICs for two rectangular rods inside the waveguide. (a) Vs distance between rectangular rods and angle of rotation, (b) vs frequency and distance between insets at $\Delta = 0$. Points of merging are marked by open circles.

planes cardinally changes the interaction between two rods to cancel L dependence.

V. TOPOLOGICALLY PROTECTED BICS MERGE INTO SP OR ACCIDENTAL BICS

Topologically protected (TP) BICs were reported by many researchers [31,54–59], which originate from the merging of several BICs in the momentum space. Very recently Huang *et al.* [60] have demonstrated TP BICs in coupled acoustic resonators, which arise from the merging of BICs in parametric space of frequency and coupling strength. The importance of the TP BICs is that they are robust to the fabrication imperfection, and that the degree of enhancement of the Q factor of quasi-BICs changes from standard quadratic to the fourth or even to the sixth degree. Here we demonstrate the cases of merging of two accidental BICs with winding numbers $m = \pm 1$ into one nonrobust accidental BIC with $m = 0$. The phase singularities arise if some complex function $\Psi(k, \phi) = u(k, \phi) + iv(k, \phi) = |\Psi(k, \phi)|\exp(i\theta(k, \phi))$ has nodal point in some two-dimensional parametric space, for example, frequency and angle of orientation (k, ϕ) or (k, Δ). Then the winding number of the singularity is given by

$$m = \mathrm{sgn}\left(\frac{\partial u}{\partial k}\frac{\partial v}{\partial \phi} - \frac{\partial u}{\partial \phi}\frac{\partial v}{\partial k}\right) \tag{1}$$

or

$$m = \oint d\vec{l}\,\nabla\theta. \tag{2}$$

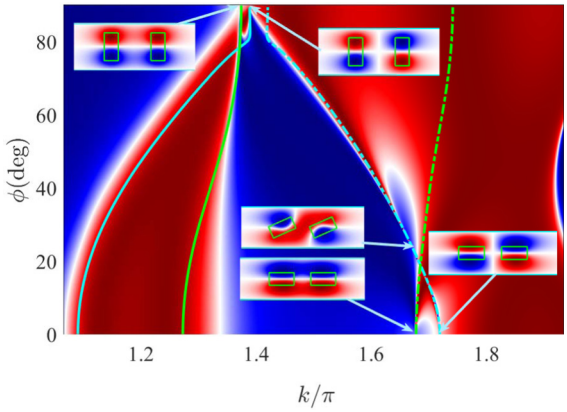

FIG. 9. Transmittance of electromagnetic waves over the waveguide vs frequency and rotation angle of rods as shown in insets. Lines show resonant frequencies as function of the rotation angle ϕ. The parameters are $a = 0.6$, $b = 0.3$, $L = 1$.

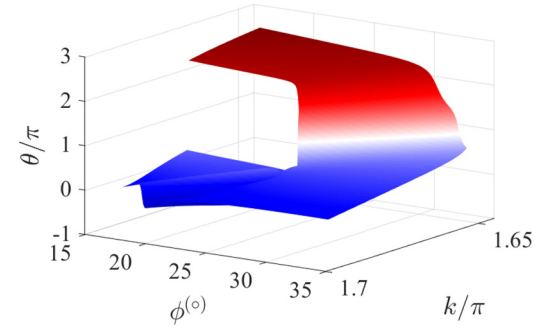

FIG. 10. The phase of function $\theta = Arg(\frac{1}{E_z})$ vs frequency and the rotation angle of dielectric rectangular rod 0.6×0.3 for the case of in-phase rotation for the parameters highlighted by open circle in Fig. 9.

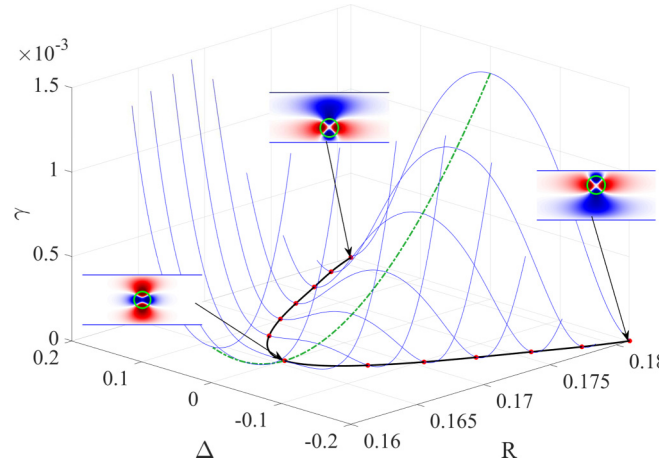

FIG. 11. Half width of resonances vs shift of cylindrical rod relative to center of waveguide and radius of rod for $n = 3.87$. Insets show patterns of BICs (E_z of electric field).

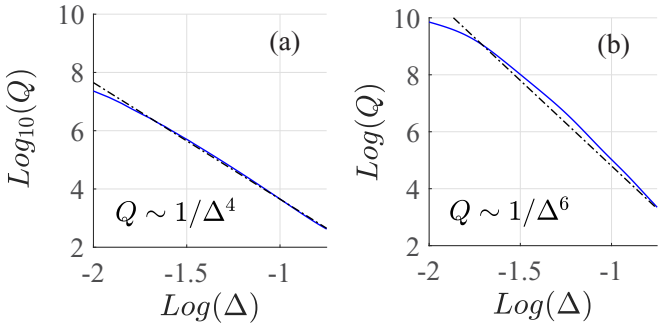

FIG. 12. Dependence of Q factor vs position of rod in waveguide in log-log scale at the points of merging of topologically protected BICs. (a) The case of circular rod shown in Fig. 11 and (b) the case of rectangular rod with cross section $a = 0.3$, $b = b_c = 0.911$ shown in Fig. 11.

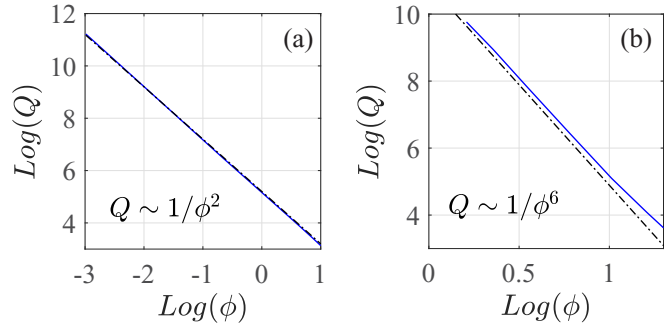

FIG. 14. Dependence of Q factor vs rotation angle of two rectangular rods with $a = 0.6, b = 0.3$ positioned symmetrically in waveguide in log-log scale at the points (a) beyond merging of topologically protected BICs marked by star in Fig. 8(b) at $L = 0.9$ and (b) at the point of merging marked by open green circle in Fig. 8(b) at $L = 0.989$.

As the parametric space we have chosen the frequency k and the angle of rotation ϕ while for the function Ψ we have chosen $\frac{1}{E_z}(x, y)$ at some fixed space point (x, y) where E_z is the zth component of electric field for the TM solution of the Maxwell equations. Figure 10 shows as the phase of this function in an anticlockwise sense, i.e., gives us $m = 1$. The merging is shown in Fig. 11 in which evolution of TP BIC with $m = \pm 1$ in two-parametric space of radius and shift of dielectric cylinder is plotted by solid-green line while the accidental BIC with $m = 0$ occurs only at $R = 0.1656$ and $\Delta = 0$.

These two TP BICs with $m = \pm 1$ are not distinguishable because are related by the inverse $y \to -y$. However, Fig. 12(a) brightly demonstrates effect of annihilation of two TP BICs which merge into the SP BIC with zero-winding number when rod with the critical radius $R_c = 0.1656$ takes the symmetrical position $\Delta \to 0$. Owing to log-log scale of dependence we obtain $Q \sim \frac{1}{\Delta^4}$. If the radius of rod were different from the critical one we would have standard quadratic behavior $Q \sim \frac{1}{\Delta^2}$. First, these phenomenon was demonstrated in periodical array of cylindrical rods in which two off-Γ BICs with winding numbers $m = \pm 1$ were merged into the SP BIC at Γ point with $m = 0$ [31]. This phenomenon is similar to the case of merging of BICs observed in the photonic system, where topological charges move toward the Γ point in first Brillouin zone at momentum space [30,54,57,61,62]. It is important to note that the merging of BICs does not mean existence of two BICs at the same point of parametric space, i.e., degeneracy of BICs. In fact, for approaching to the merging point accidental BICs vanish compared to the SP BIC.

Figure 13 demonstrates similar effects for the case of rectangular rod $a \times b$ in two-parametric space of length a and position Δ. At the merging point of two TP BICs with SP BIC the behavior of Q factor turns into $Q \sim \frac{1}{\Delta^6}$ as shown in Fig. 12 (b).

The case of two rectangular rods brings a novelty of the merging of three BICs, two Fabry-Perot BICs with winding numbers $m = \pm 1$ and one SP BIC with $m = 0$. Beyond the point of merging [marked by star in Fig. 8(b)] we have standard quadratic behavior of the Q factor as demonstrated in Fig. 14(a). However, at the points of merging marked by open circles in Fig. 8(b) we obtain strong dependence $Q \sim \frac{1}{\Delta^6}$ as Fig. 14(b) shows.

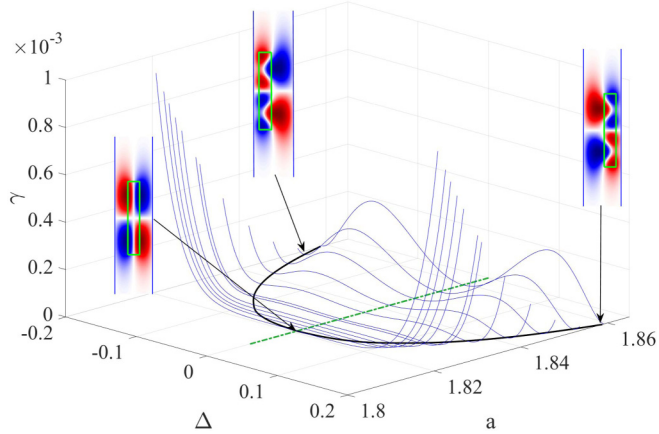

FIG. 13. Half width of resonances vs shift of rectangular rod $a \times b$ with $n = 2.05$ and length a at $b = 0.3$. Insets show patterns of BICs (E_z of electric field).

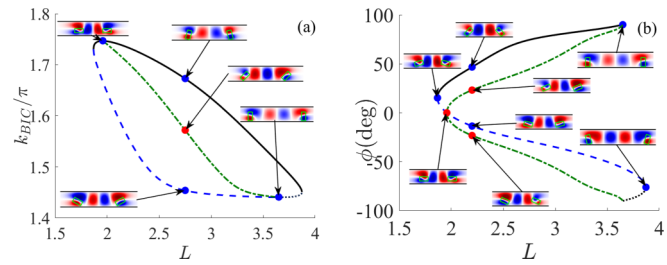

FIG. 15. Curves of existence of the Fabry-Perot BICs vs (a) distance between rectangular rods and frequency and (b) angle of rotation and distance between rods at $\Delta = 1/2$. Dash-dotted lines show curves of Fabry-Perot SP BICs at $\phi = 0, 90°$. Green-solid line and dash-gray lines show topologically protected in-phase BICs and antiphase BICs, respectively. Points of BICs merging are marked by open circles.

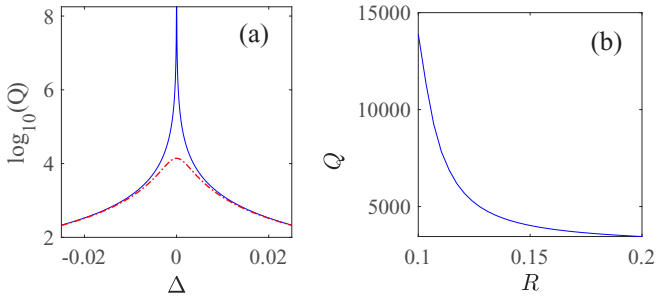

FIG. 16. Dependence of frequency (a) and the Q factor (b) of the SP quasi BIC vs radius of Si rod in the GHz range with account of material losses of rod.

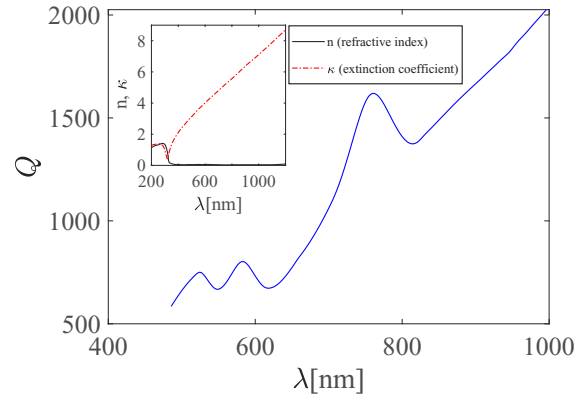

FIG. 17. Dependence of Q factor of the SP quasi-BIC vs wavelength for the rod integrated into silver waveguide in the optical range with account of surface impedance of silver.

Crossover of the degree of enhancement of the Q factor is related to bifurcation of imaginary parts of TP BICs as Figs. 11 and 13 show. That result follows from the algebra of bifurcation [31,57,60,62,63].

One can see in Fig. 8 points in which SP BICs at $\phi = 0, 90^o$ (dash-dot blue lines) coalesce with Fabry-Perot BICs evolving with angle of in phase or antiphase rotation of rods shown by solid-green and dash-gray lines. These Fabry-Perot BICs have morphology cardinally different from the SP BICs as seen from insets in Fig. 8. For each angle $\phi \neq 0$ the Fabry-Perot BIC has to be tuned by distance between rods L making an analogy with accidental BICs. Figure 15 demonstrates rich variety of merging effects of BICs with different winding numbers in the three-parametric space of frequency, distance between the rectangular rods and rotation angle.

VI. CONCLUSIONS AND DISCUSSION

A simple system of plane waveguide consisted of two parallel metal planes with integrated one or two dielectric quartz or silicon rods demonstrates abundance of various BICs classified as symmetry protected (SP), accidental, Friedrich-Wintgen and Fabry-Perot. Moreover, we show numerous points of merging of different topologically protected BICs in two-parametric space. These events give rise to change of the power degree in asymptotic behavior of the Q factor that has principal importance for numerous applications of BICs. First, this phenomenon of BICs merging was observed in the photonic system, where topological charges move toward the Γ point in first Brillouin zone at momentum space [30,54,57,61,62]. Quite recently the two-parametric space was expanded onto the frequency and coupling strength of two acoustic resonators [60]. In the present paper we go further by introducing parameters determining position of rods, distance between them, orientation of rectangular shaped rods, and frequency. It is important that all parameters can be easily varied experimentally in comparison to the case of topologically protected BICs in momentum space in the one- and two-dimensional periodical arrays of dielectric particles. It is clear that one can consider three-parametric space in which we can observe the lines of TP BICs.

Finally, we discuss the extend to which extend the present system of plane metallic waveguide with integrated dielectric rod is preferable compared to periodic array of rods with account of material losses. The comparison crucially depends on the frequency range in which BICs are supposed to be observed. For example, the Q factor of SP BICs in the GHz range in the array of ceramic disks is saturated by a value 4000 [17]. While the array of Si disks with $\tan\delta = 4 \times 10^{-4}$ we have $Q_{max} = 2500$. In this range the silver surface can be considered as perfectly conducting material, and therefore the main contribution is due to material losses of rod integrated into waveguide. Figure 16 presents results of COMSOL Multiphysics computations, which show the frequency of SP BICs and its Q factor versus the radius of rod that shows considerable gain of the present system compared to the periodical array of rods in the GHz range.

In the optical range the main adverse factor is the surface impedance of silver metal that considerably restricts the Q factor as shown in Fig. 17 by use of data of Ref. [64]. Nevertheless (in the range of red line in the figure) the Q factor of the SP BIC can exceed a value 2000.

ACKNOWLEDGMENTS

We are grateful to Lujun Huang, Andrey Miroshnichenko and Yi Xu for presentation of unpublished paper [60] and discussions. The research was supported by Russian Science Foundation No. 22-12-00070.

[1] G. Mie, Beiträge zur optik trüber medien, speziell kolloidaler metallösungen, Ann. Phys. **330**, 377 (1908).

[2] J. D. Joannopoulos, S. G. Johnson, J. N. Winn, and R. D. Meade, *Photonic Crystals: Molding the Flow of Light* (Princeton University Press, Princeton, NJ, 1995)

[3] P. Vincent and M. Nevi'ere, Corrugated dielectric waveguides: A numerical study of the second-order stop bands, Appl. Phys. **20**, 345 (1979).

[4] A.-S. Bonnet-Bendhia and F. Starling, Guided waves by electromagnetic gratings and non-uniqueness examples for

the diffraction problem, Math. Meth. Appl. Sci. **17**, 305 (1994).

[5] V. Astratov, J. Culshaw, R. Stevenson, D. Whittaker, M. Skolnick, T. Krauss, and R. de la Rue, Resonant coupling of near-infrared radiation to photonic band structure waveguides, J. Light. Technol. **17**, 2050 (1999).

[6] S. G. Tikhodeev, A. L. Yablonskii, E. A. Muljarov, N. A. Gippius, and T. Ishihara, Quasiguided modes and optical properties of photonic crystal slabs, Phys. Rev. B **66**, 045102 (2002).

[7] S. P. Shipman and S. Venakides, Resonant transmission near nonrobust periodic slab modes, Phys. Rev. E **71**, 026611 (2005).

[8] D. C. Marinica, A. G. Borisov, and S. V. Shabanov, Bound States in the Continuum in Photonics, Phys. Rev. Lett. **100**, 183902 (2008).

[9] C. W. Hsu, B. Zhen, J. Lee, S. G. Johnson, J. D. Joannopoulos, and M. Soljačić, Observation of trapped light within the radiation continuum, Nature (London) **499**, 188 (2013).

[10] E. N. Bulgakov and A. F. Sadreev, Bloch bound states in the radiation continuum in a periodic array of dielectric rods, Phys. Rev. A **90**, 053801 (2014).

[11] Y. Yang, C. Peng, Y. Liang, Z. Li, and S. Noda, Analytical Perspective for Bound States in the Continuum in Photonic Crystal Slabs, Phys. Rev. Lett. **113**, 037401 (2014).

[12] D. Bykov and L. Doskolovich, $\omega - kx$ Fano line shape in photonic crystal slabs, Phys. Rev. A **92**, 013845 (2015).

[13] Z. Hu and Y. Y. Lu, Standing waves on two-dimensional periodic dielectric waveguides, J. Opt. **17**, 065601 (2015).

[14] C. W. Hsu, B. Zhen, S.-L. Chua, S. G. Johnson, J. D. Joannopoulos, and M. Soljačić, Bloch surface eigenstates within the radiation continuum, Light Sci. Appl. **2**, e84 (2013).

[15] X. Gao, C. W. Hsu, B. Zhen, X. Lin, J. D. Joannopoulos, M. Soljačić, and H. Chen, Formation mechanism of guided resonances and bound states in the continuum in photonic crystal slabs, Sci. Rep. **6**, 31908 (2016).

[16] Z. F. Sadrieva, I. S. Sinev, K. L. Koshelev, A. Samusev, I. V. Iorsh, O. Takayama, R. Malureanu, A. A. Bogdanov, and A. V. Lavrinenko, Transition from optical bound states in the continuum to leaky resonances: Role of substrate and roughness, ACS Photonics **4**, 723 (2017).

[17] Z. F. Sadrieva, M. A. Belyakov, M. A. Balezin, P. V. Kapitanova, E. A. Nenasheva, A. F. Sadreev, and A. A. Bogdanov, Experimental observation of a symmetry-protected bound state in the continuum in a chain of dielectric disks, Phys. Rev. A **99**, 053804 (2019).

[18] E. Maslova, M. Rybin, A. Bogdanov, and Z. Sadrieva, Bound states in the continuum in periodic structures with structural disorder, Nanophotonics **10**, 4313 (2021).

[19] M. V. Rybin, K. L. Koshelev, Z. F. Sadrieva, K. B. Samusev, A. A. Bogdanov, M. F. Limonov, and Y. S. Kivshar, High-Q Supercavity Modes in Subwavelength Dielectric Resonators, Phys. Rev. Lett. **119**, 243901 (2017).

[20] A. Bogdanov, K. Koshelev, P. Kapitanova, M. Rybin, S. Gladyshev, Z. Sadrieva, K. Samusev, Y. Kivshar, and M. F. Limonov, Bound states in the continuum and Fano resonances in the strong mode coupling regime, Adv. Photonics **1**, 016001 (2019).

[21] K. Koshelev, G. Favraud, A. Bogdanov, Y. Kivshar, and A. Fratalocchi, Nonradiating photonics with resonant dielectric nanostructures, Nanophotonics **8**, 725 (2019).

[22] M. Odit, K. Koshelev, S. Gladyshev, K. Ladutenko, Y. Kivshar, and A. Bogdanov, Observation of supercavity modes in subwavelength dielectric resonators, Adv. Mater. **33**, 2003804 (2020).

[23] L. Huang, L. Xu, M. Rahmani, D. Neshev, and A. Miroshnichenko, Pushing the limit of high-Q mode of a single dielectric nanocavity, Adv. Photonics **3**, 016004 (2021).

[24] E. Bulgakov, K. Pichugin, and A. Sadreev, Mie resonance engineering in two disks, Photonics **8**, 49 (2021).

[25] K. Pichugin, A. Sadreev, and E. Bulgakov, Ultrahigh-Q system of a few coaxial disks, Nanophotonics **10**, 4341 (2021).

[26] D. Colton and R. Kress, *Inverse Acoustic and Electromagnetic Scattering Theory*, 2nd ed. (Springer, Berlin, 1998).

[27] M. G. Silveirinha, Trapping light in open plasmonic nanostructures, Phys. Rev. A **89**, 023813 (2014).

[28] K. Koshelev, A. Bogdanov, and Y. Kivshar, Meta-optics and bound states in the continuum, Sci. Bull. **64**, 836 (2019).

[29] W. Chen, Y. Chen, and W. Liu, Multipolar conversion induced subwavelength high-Q Kerker supermodes with unidirectional radiations, Laser Photonics Rev. **13**, 1900067 (2019).

[30] L. Yuan and Y. Y. Lu, Bound states in the continuum on periodic structures: perturbation theory and robustness, Opt. Lett. **42**, 4490 (2017).

[31] E. N. Bulgakov and D. N. Maksimov, Bound states in the continuum and polarization singularities in periodic arrays of dielectric rods, Phys. Rev. A **96**, 063833 (2017).

[32] E. Bulgakov and D. Maksimov, Light enhancement by quasi-bound states in the continuum in dielectric arrays, Opt. Express **25**, 14134 (2017).

[33] L. Yuan and Y. Y. Lu, Bound states in the continuum on periodic structures surrounded by strong resonances, Phys. Rev. A **97**, 043828 (2018).

[34] D. R. Abujetas, J. J. Sáenz, and J. A. Sánchez-Gil, Narrow Fano resonances in Si nanocylinder metasurfaces: Refractive index sensing, J. Appl. Phys. **125**, 183103 (2019).

[35] Z. Hu, L. Yuan, and Y. Y. Lu, Resonant field enhancement near bound states in the continuum on periodic structures, Phys. Rev. A **101**, 043825 (2020).

[36] Z. Hu, L. Yuan, and Y. Y. Lu, Bound states with complex frequencies near the continuum on lossy periodic structures, Phys. Rev. A **101**, 013806 (2020).

[37] R. F. Ndangali and S. Shabanov, Electromagnetic bound states in the radiation continuum for periodic double arrays of subwavelength dielectric cylinders, J. Math. Phys. **51**, 102901 (2010).

[38] M. S. Sidorenko, O. N. Sergaeva, Z. F. Sadrieva, C. Roques-Carmes, P. S. Muraev, D. N. Maksimov, and A. A. Bogdanov, Observation of an accidental bound state in the continuum in a chain of dielectric disks, Phys. Rev. Applied **15**, 034041 (2021).

[39] D. V. Evans, M. Levitin, and D. Vassiliev, Existence theorems for trapped modes, J. Fluid Mech. **261**, 21 (1994).

[40] D. V. Evans and R. Porter, Trapped modes embedded in the continuous spectrum, Q. J. Mech. Appl. Math. **51**, 263 (1998).

[41] J. N. Newman, Trapped-wave modes of bodies in channels, J. Fluid Mech. **812**, 178 (2017).

[42] C. Linton, M. McIver, P. McIver, K. Ratcliffe, and J. Zhang, Trapped modes for off-centre structures in guides, Wave Motion **36**, 67 (2002).

[43] Y. Duan, W. Koch, C. Linton, and M. Mciver, Complex resonances and trapped modes in ducted domains, J. Fluid Mech. **571**, 119 (2007).

[44] A. Overvig, S. Shrestha, and N. Yu, Dimerized high contrast gratings, Nanophotonics **7**, 1157 (2018).

[45] Q. Song, M. Zhao, L. Liu, J. Chai, G. He, H. Xiang, D. Han, and J. Zi, Observation of bound states in the continuum in the dimerized chain, Phys. Rev. A **100**, 023810 (2019).

[46] K. Yasumoto and H. Jia, Modeling of photonic crystals by multilayered periodic arrays of circular cylinders, in *Electromagnetic Theory and Applications for Photonic Crystals*, edited by K. Yasumoto (MIT Press, Cambridge, MA, 2006), pp. 527–579.

[47] T. Kushta and K. Yasumoto, Electromagnetic scattering from periodic arrays of two circular cylinders per unit cell, Prog. Electromagn. Res. **29**, 69 (2000).

[48] A. F. Sadreev, Interference traps waves in an open system: Bound states in the continuum, Rep. Prog. Phys. **84**, 055901 (2021).

[49] C. S. Kim, A. M. Satanin, Y. S. Joe, and R. M. Cosby, Resonant tunneling in a quantum waveguide: Effect of a finite-size attractive impurity, Phys. Rev. B **60**, 10962 (1999).

[50] V. Liu, M. Povinelli, and S. Fan, Resonance-enhanced optical forces between coupled photonic crystal slabs, Opt. Express **17**, 21897 (2009).

[51] A. F. Sadreev, E. N. Bulgakov, and I. Rotter, Bound states in the continuum in open quantum billiards with a variable shape, Phys. Rev. B **73**, 235342 (2006).

[52] H. Chen, H. Wang, K. yin Wong, and D. Lei, High-Q localized surface plasmon resonance based on bound states in the continuum for enhanced refractive index sensing, Opt. Lett. **47**, 609 (2022).

[53] E. N. Bulgakov, K. N. Pichugin, and A. F. Sadreev, Evolution of the resonances of two parallel dielectric cylinders with distance between them, Phys. Rev. A **100**, 043806 (2019).

[54] E. N. Bulgakov and D. N. Maksimov, Topological Bound States in the Continuum in Arrays of Dielectric Spheres, Phys. Rev. Lett. **118**, 267401 (2017).

[55] S. Mukherjee, J. Gomis-Bresco, P. Pujol-Closa, D. Artigas, and L. Torner, Topological properties of bound states in the continuum in geometries with broken anisotropy symmetry, Phys. Rev. A **98**, 063826 (2018).

[56] W. Liu, B. Wang, Y. Zhang, J. Wang, M. Zhao, F. Guan, X. Liu, L. Shi, and J. Zi, Circularly Polarized States Spawning from Bound States in the Continuum, Phys. Rev. Lett. **123**, 116104 (2019).

[57] J. Jin, X. Yin, L. Ni, M. Soljačić, B. Zhen, and C. Peng, Topologically enabled ultrahigh-q guided resonances robust to out-of-plane scattering, Nature (London) **574**, 501 (2019).

[58] T. Yoda and M. Notomi, Generation and Annihilation of Topologically Protected Bound States in the Continuum and Circularly Polarized States by Symmetry Breaking, Phys. Rev. Lett. **125**, 053902 (2020).

[59] M.-S. Hwang, H.-C. Lee, K.-H. Kim, K.-Y. Jeong, S.-H. Kwon, K. Koshelev, Y. Kivshar, and H.-G. Park, Ultralow-threshold laser using super-bound states in the continuum, Nat. Commun. **12**, 4135 (2021).

[60] L. Huang, B. Jia, Y. K. Chiang, S. Huang, C. Shen, F. Deng, T. Yang, D. Powell, Y. Li, and A. Miroshnichenko, Topological supercavity resonances in the finite system, Adv. Sci. **9**, 2200257 (2022).

[61] B. Zhen, C. W. Hsu, L. Lu, A. D. Stone, and M. Soljačić, Strong Resonances on Periodic Arrays of Cylinders and Optical Bistability with Weak Incident Waves, Phys. Rev. Lett. **113**, 257401 (2014).

[62] Y. Zeng, G. Hu, K. Liu, Z. Tang, and C.-W. Qiu, Dynamics of Topological Polarization Singularity in Momentum Space, Phys. Rev. Lett. **127**, 176101 (2021).

[63] L. Yuan and Y. Y. Lu, Strong resonances on periodic arrays of cylinders and optical bistability with weak incident waves, Phys. Rev. A **95**, 023834 (2017).

[64] P. B. Johnson and R. W. Christy, Optical constants of the noble metals, Phys. Rev. B **6**, 4370 (1972).